Laser Powered Homogeneous Pyrolysis (LPHP) of Lignin Dispersed into Gas-Phase

Mohamad Mohamad Barekati-Goudarzi , Lavrent Khachatryan , Rubik Asatryan * , Dorin Boldor , Bert Lynn

Posted Date: 8 April 2025

doi: 10.20944/preprints202504.0455.v1

Keywords: PAH; lignin pyrolysis; laser reactor; depolymerization; soot; radicals

 doi:10.20944/preprints202504.0455.v1

Article

Laser Powered Homogeneous Pyrolysis (LPHP) of Lignin Dispersed into Gas-phase

Mohamad Barekati-Goudarzi [1], Lavrent Khachatryan [1], Rubik Asatryan [2,*], Dorin Boldor [3] and Bert C. Lynn [4]

[1] Department of Chemistry, Louisiana State University, Baton Rouge, Louisiana 70803, USA
[2] Department of Chemical and Biological Engineering, University at Buffalo, The State University of New York, Buffalo, NY 14260, USA
[3] Department of Biological & Agricultural Engineering, LSU, and LSU AgCenter, Baton Rouge, Louisiana 70803, USA
[4] Department of Chemistry, University of Kentucky, Lexington, Kentucky 40506, USA
* Correspondence: rubikasa@buffalo.edu

Abstract: The gas phase delivery of lignin into the hot zone of cw-CO_2 laser powered homogeneous pyrolysis (LPHP) reactor under "wall-less" conditions led to break down of lignin macromolecules into neutral oligomers and paramagnetic fragments deposited onto the reactor cell walls. Formation of PAHs was observed during defragmentation of lignin accelerated with increased laser power. Remarkably, no phenolic compounds were detected among lignin fragments - intermediate radicals and neutral oligomers. It is concluded that the PAH and soot-like conjugated particulates are formed in the hot zone of the LPHP reactor resembling the high temperature combustion processes. The key role of the resonantly stabilized radicals in the formation of low molecular weight PAHs is outlined. An alternative pathway is proposed for generation of PAH involving formation of cyclopentadienyl radical precursors (CPDa) that are adsorbed onto or trapped within lignin macromolecules.

Keywords: PAH; lignin pyrolysis; laser reactor; depolymerization; soot; radicals

1. Introduction

Understanding and monitoring the production of bio-oils by fast biomass pyrolysis is an efficient way to optimize the involved chemical processes and improve their subsequent refinement. To bypass intractable secondary processes during solid phase pyrolysis of lignin, we have recently introduced a straightforward approach involving initial gasification of lignin macromolecules. Lignin dissolved in a solution of acetone/water (9:1 ratio) has been pulverized into gas phase in a contactless, tubular reactor [1,2]. The overall goal of the experiments was to limit the side effects typically accompanying pyrolysis of solid-state lignin in conventional reactors. Depending on the delivery modes, two different types of reactors were utilized: 1) Continuous Droplet Evaporation (CDE), and 2) Constant output Atomization (CA) reactors. Lignin was transported through the isothermal zone by either syringe pump (CDE reactor) or TSI atomizer (CA reactor). The results revealed new features for degradation of hydrolytic lignin (HL) dispersed into the gas phase compared to those in the conventional batch reactors. In particular, the formation of intermediate oligomers in both reactors were shown to occur involving only trace amounts of phenolic compounds [1,2].

Some preliminary results on pyrolysis of lignin in the gas-phase using a "wall-less", cw-IR CO_2 Laser Powered Homogeneous Pyrolysis (LPHP) non-isothermal reactor was briefly reported elsewhere [3,4]. The temperature distribution in the LPHP reactor was monitored by thermocouple measurements validated by the method of "chemical thermometer" and COMSOL Multiphysics simulations [3,4]. Large differences were found between the gas phase depolymerization of lignin in

 doi:10.20944/preprints202504.0455.v1

the LPHP reactor and conventional reactors, yet much similarity was seen with CDE and CA reactors. The gas phase delivery of lignin into the hot zone of the LPHP reactor under "wall-less" conditions led to the break-down of lignin into neutral and paramagnetic fragments that deposited onto the cell walls [3]. Because of the steep/narrow temperature zone in the center of the LPHP reactor, these fragments readily leave the hot zone and quench/stabilize in the cold areas of the reactor primarily on the cold walls.

No phenolics were detected in LPHP reactor, instead the formation of polycyclic aromatic hydrocarbons (PAHs) was observed, and the yields of PAHs accelerated with increasing laser power. Understanding underlying chemistry of PAHs formation observed virtually in any biomass conversion and combustion process, [5,6] presents a significant challenge. Here, we attempt to address this issue. While PAHs are typically perceived as toxic and unwanted byproducts of biomass pyrolysis, they could serve as biomass-derived precursors for valuable carbon-based materials, including carbon fibers, films, and bio-coal. [7]. In particular, the inclusion of small quantities of low molecular weight PAHs as additives in diesel fuel enhances the physicochemical properties of diesel surrogate fuel blends, leading to improvements in both energy density and viscosity [8,9].

Note that the accumulation of PAHs in the conventional reactors, as detailed in [10] tends to increase with temperature. However, a critical decrease is observed in the yields of PAHs containing two fused aromatic rings. This insight is essential for regulating the composition of PAH mixtures based on temperature variations.

The associative chemical gas-phase reactions of radical fragments by selective formation of low molecular weight aromatic hydrocarbons (LMW PAHs having molecular weight less than 300g/mol and detectable by GC-MS) are discussed in the current work along with the combustion related processes leading to the formation of "younger" soot macromolecules which may occur in the hot zone in LPHP reactor. These chemical processes provide additional evidence for breakdown of the lignin macromolecules into intermediate fragments (neutral and radical oligomers) we have shown previously to occur in different pyrolysis reactors. [1–3]

2. Experimental

2.1. Materials

Hydrolytic lignin (HL) was purchased from Sigma-Aldrich (a currently discontinued product, 37-107-6). This product mostly contains low molecular weight oligomers (<500 Da), i.e. dimers containing four oxygen atoms ($C_{18}H_{18}O_4$) and trimers with six oxygen atoms ($C_{27}H_{26}O_6$), with a weight percent ratio of C/H/O that equals 76:6:18 [11]. Lignin was fractionated by molecular sieves from mesh #60-120, and the fraction of #100-120 was used in this study (125 μm ≤ nominal size ≤ 149 μm). The hydrolytic lignin was well dissolved using vortex stirrer followed by 30 min of sonication in acetone/water (9:1 volume ratio) mixture. This solution was then atomized in the gas phase by a constant output TSI 3076 atomizer into the pyrolysis reactor (refer [1,2] for details).

2.2. IR Laser Powered Homogeneous Pyrolysis (LPHP) Reactor

The general features of the LPHP reactor, which facilitate the homogeneous pyrolysis of organic compounds, are described in detail elsewhere. [3,4]. The schematic of the IR LPHP reactor, which is irradiated from the side window by IR CO_2 laser, is represented in Figure S1. A continuous wave cw-CO_2 laser source was used at the P (20) line of the 00°1 → 10°0 transition (10.59 μm) with a maximum output of 40 W (Synrad Firestar CO_2 laser, FSV40KWD). A set of highly transparent KBr disks to the CO_2 laser irradiation (10.6 μm) were used as an entry window for laser reactor cell. The reactor is a Pyrex glass tube (i.d. = 20 mm, length = 10 cm) fitted from both sides with KBr windows. To avoid the destructive effect of moisture on the hygroscopic window material, as well as the deposition of expected heavy intermediates from HL pyrolysis on the surfaces of both windows, they were protected by direct flow of N_2 through the reaction cell close to the windows, Figure S1. The laser energy is absorbed by the sensitizer gas SF_6, which is mixed with the initial flow of the lignin

 doi:10.20944/preprints202504.0455.v1

dispersed into N_2 carrier gas and rapidly transferred to the ambient gas and reactants. An important characteristic of SF_6 is its general non-reactivity, *i.e.* it does not pyrolyze significantly below 1350°C [12]. The secondary tar-forming reactions are limited in the LPHP reactor because of the sharp temperature drop on the border of the hot volume reaction zone and the corresponding drastic decrease of the chain-propagation reaction rates[3]. In other words, the extremely pronounced temperature drop from the central axis of the LPHP reactor toward the surrounding areas have a quite different effect on the various reaction steps in comparison with a conventionally heated tube reactor, as it has been shown in a number of earlier publications [12–18].

The details of the results obtained from the standard analytical techniques, namely GC-MS, EPR, FTIR, GPC, are presented in Supporting Information.

3. Results and Discussion

LPHP countercurrent reactor: The countercurrent design reactor was placed in an isothermal reactor, Figure 1 (refer LPHP co-current reactor in supporting information, inset in Figure S2); the wall temperature was maintained at 300°C to avoid condensation/deposition on the cold walls of reactor. Most deposits were easily collected from the neck of the sampling port, and, at the same time, analysis of the condensable gases trapped at -196 °C could be undertaken. This reactor is made from Pyrex with 20 cm length of heated wall using an electric furnace. The unique countercurrent design with various tube sizes (I.D.= 6, 11, and 20 mm), as well as the side injection of the N_2 gas ensured the confinement of the reactive hot zone in the target zone. Dispersed hydrolytic lignin in gas phase was provided by a commercially available TSI 3076 Constant Output atomizer operated at 3-5 L/min flowrate, and a 2% SF_6 was provided in the N_2 gas mixture.

Due to the complexity of the direct temperature measurements, computational numerical modeling was undertaken to simulate and identify the temperature distribution in the reactor. COMSOL Multiphysics (v5.3a, COMSOL Inc, Burlington, MA), a finite element analysis (FEA) software package, was used to solve the ordinary differential equations (ODEs) and partial differential equations (PDEs) involved in the laser light absorption and transition into heat transfer in the fluid as well as fluid dynamic models, using a procedure modified in our previous work [4]. The initial phase of computational temperature measurements along with the experimental validation for a similar system can be found elsewhere [3].

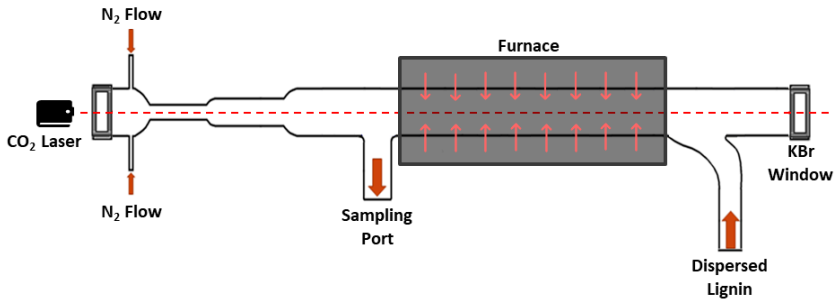

Figure 1. Schematic of the IR countercurrent LPHP reactor.

3.1. Temperature Distribution in LPHP Countercurrent Reactor

The temperature profiles inside the LPHP reactor based on COMSOL Multiphysics simulation are mapped in Figure 2. For these calculations, three types of mesh (coarse, normal, and fine mesh) were studied with respect to the efficiency of simulation and accuracy of the results.

As expected, by elevating the laser power, the temperature of the hot zone increases and propagates into a longer distance at the onset of absorption. The laser beam has a 2.5 mm diameter where the maximum radial temperature is calculated. Considering a volume with temperature above 400 °C as the reacting zone for each laser power, the calculated residence time of the lignin in the hot zone, for a 3 L/min carrier gas flowrate, can be evaluated to range from 40 ms to 160 ms,

 doi:10.20944/preprints202504.0455.v1

corresponding to the 14.7 W to 38 W laser power, respectively. The high maximum temperature shown on Figure 2 for each laser power can compensate for such a short residence time to achieve reasonable conversion rates. Note, the TSI 3076 Constant Output Atomizer generates extremely fine aerosols with number mean droplet diameter of 0.30 μm from the lignin solution, ideal to be rapidly heated to the temperature achieved in the hot zone. Moreover, the steep temperature profile achieved in this reactor and fast cooling of pyrolysis products provide great conditions for obtaining the primary products or preserving intermediates emerging from lignin pyrolysis.

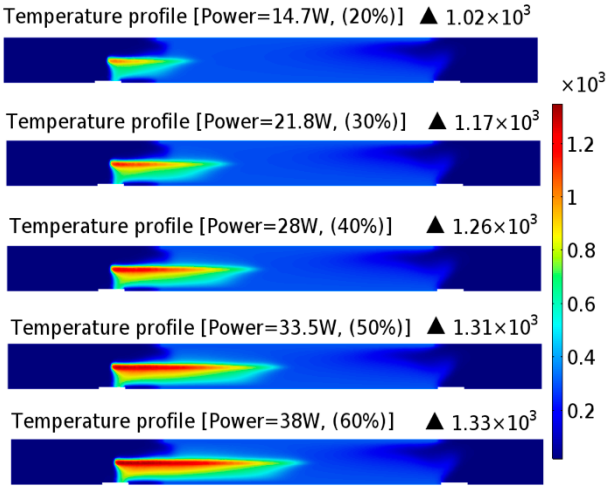

Figure 2. COMSOL prediction of the "hot zone" temperature shown on a cross sectional plane along axial direction (Z coordinate) at 14.7, 21.8, 28, 33.5, 38 W laser power with a 2% SF6 in N2 gas mixture at atmospheric condition.

3.2. *Condensable Products from Countercurrent LPHP Reactor*

The GC-MS results from countercurrent LPHP reactor are represented in Figure 3 (the products identifications is provided in Tables S1–S4, supporting information) at different laser powers from 14.7 to 38 W. The products condensed in the cold trap were extracted with acetone at the end of experiment and analyzed by GC-MS.

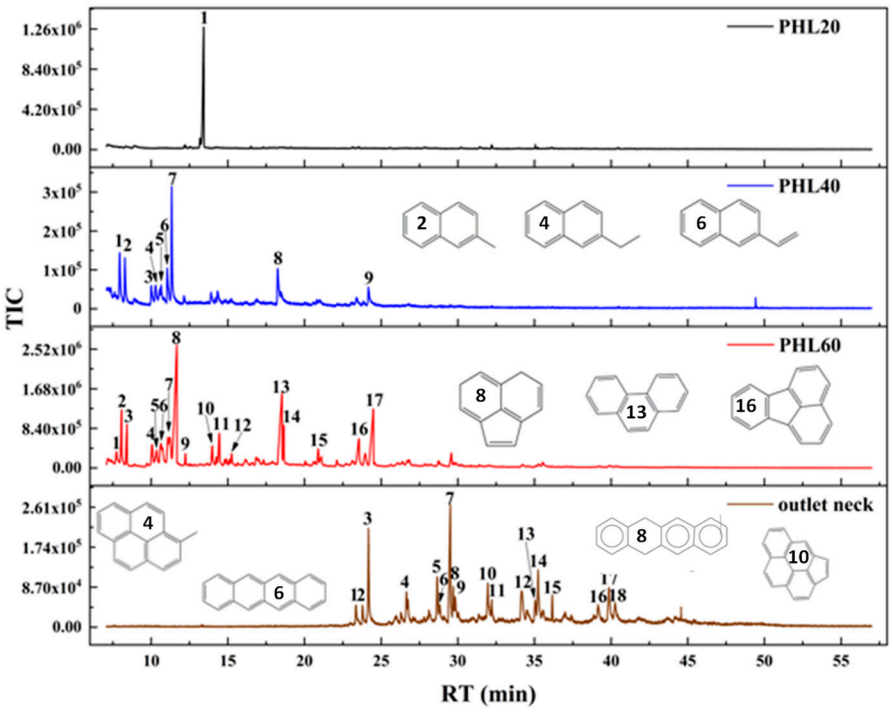

 doi:10.20944/preprints202504.0455.v1

Figure 3. GC-MS chromatograms of the products of the homogeneous pyrolysis of lignin in counter-current LPHP reactor (Figure 1) at various laser powers and locations in the reactor. HL mass transfer rate ~ 2.5 μg/s, residence time 100 ms, outside reactor temperature 300°C. The products identifications in Tables S1-S4 (supporting information). The laser power assignments PHL 20, 40, 60 stands for pyrolyzed hydrolytic lignin (PHL) at laser power of 20% (14.7W), 40% (28 W), 60% (38 W). #1 compound at PHL20 is guaiacol which most probably formed from vinyl guaiacol; the latter one is an intrinsic compound in HL.

Surprisingly, no phenolics (phenols, guaiacols, syringols, etc.) were detected in noticeable amounts. Different fused aromatic rings containing PAHs were detected with increasing laser power at ascending order of aromatic rings in PAHs, Figure 3, (Tables S1–S4, supporting information). Notably, the PAHs were not detected below 22 W laser power.

The formation of PAHs was also identified by FTIR analysis of trapped products from sampling port of LPHP reactor; the frequency at 726 cm^{-1} being a characteristic vibration mode for the C–H wags in an aromatic ring in fused ring systems, Figure 4 (at PHL 40, PHL 60; refer the abbreviations in Figure 4 caption). These peaks, however, are missing in FTIR spectra of deposited products on the outlet neck and top wall of the reactor, Figure 4. In other words, the emergence of the strong peak at 726 cm^{-1} (spectra at PHL 40, PHL 60, Figure 4), due to the C–H wags for an aromatic ring with 3, 4 and 5 adjacent hydrogen atoms, indicates the formation of fused ring systems, such as substituted naphthalene, anthracene, or phenanthrene. These compounds were abundant among products trapped during pyrolysis at high laser power.

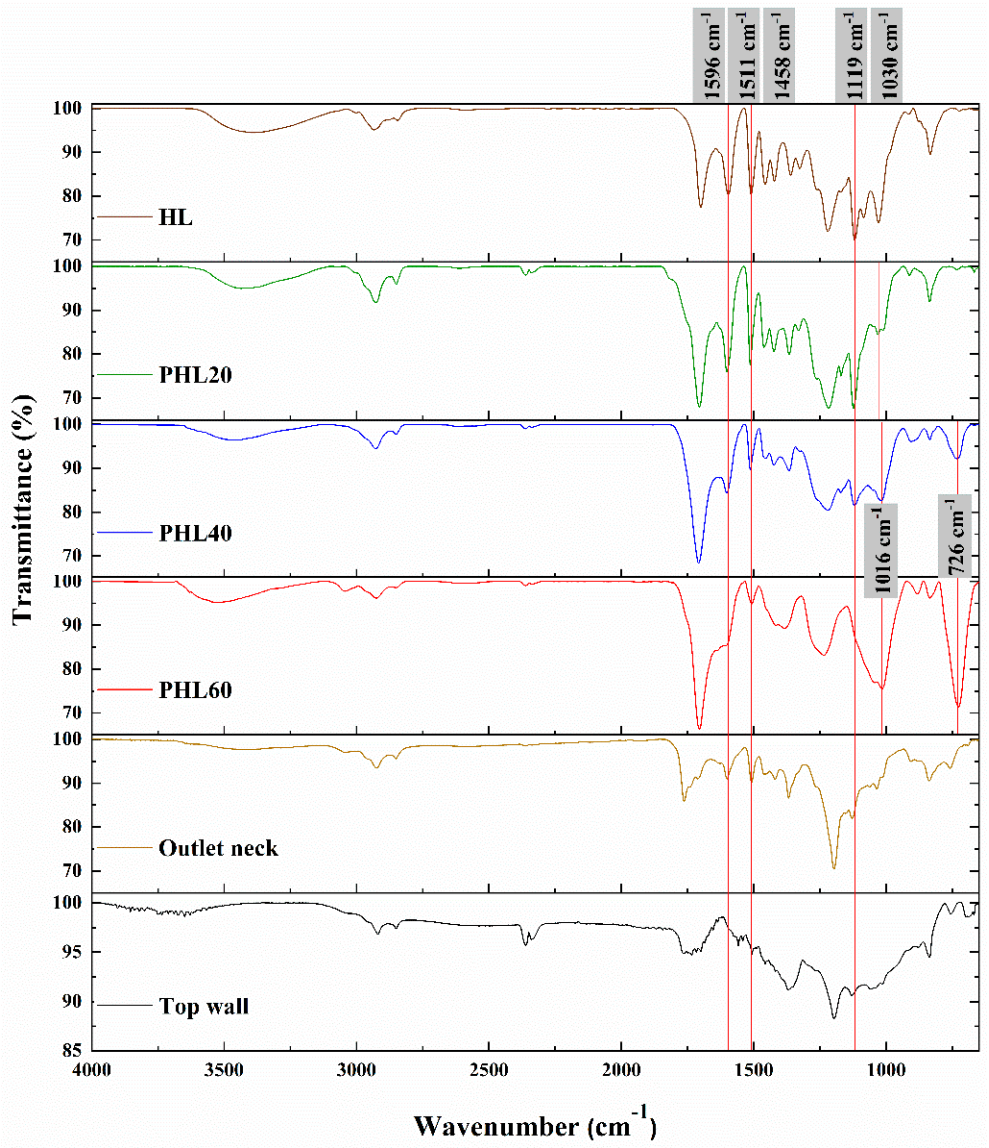

 doi:10.20944/preprints202504.0455.v1

Figure 4. FTIR spectra of the condensed products in the trap from lignin homogeneous pyrolysis in LPHP reactor at laser power of 20% (14.7W), 40% (28 W), 60% (38 W) as well as the deposited products on the outlet neck and top wall. PHL – pyrolyzed HL.

A detailed peak identification of the FTIR spectra is presented in Table 1. It is obvious that as the energy of the laser increases, the major aromatic structural units in the lignin macromolecules, labeled as the most characteristic bands at 1596 and 1511 cm^{-1}, and 1119 and 1030 cm^{-1} for C=C and C–H vibration in skeletal aromatic ring, break down, Figure 4.

Table 1. FTIR characteristics of the analyzed samples.

Wavenumber (cm^{-1})	Peak Assignment
3394	O–H stretching in hydroxyl groups in phenolic and aliphatic structures [19,20]
2936	C–H stretching in methoxy, methyl and methylene [19]
2846	C=O stretching in p-substituted aryl ketones [19]
1700	C=C stretching in aromatic ring (S) [19]
1596	C=C stretching in skeletal aromatic ring (S>G) [20,21]
1511	C=C stretching in skeletal aromatic ring (G>S) [20,21]
1458	C–H bending in methoxy and methylene [20]
1422	C–H in-plane deformation combined with skeletal aromatic ring [20]
1367	O–H in-plain bending [21]; O–H in phenol, aliphatic C–H stretch in CH_3 [20]
1326	C–H bending in aromatic ring (S or condensed G) [20]
1220	Aryl–O of aryl–OH and aryl–OCH_3 [20]
1119	C–H bending in aromatic ring (S> condensed G) [20]
1085	C–O deformation in secondary alcohols and aliphatic ethers [20]
1030	C–O stretch in O–CH_3 and C–OH [21]
915	C–H out-of-plane deformation of aromatic ring [20]
834	C–H out-of-plane in H unit and $C_{2,6}$ of S unit [20]
726	C–H wags for an aromatic fused ring [21]

Demethoxylation constitutes another phenomenon that is intensified when temperature is increased observed from the FTIR spectra. Bands at 1458, 1085 and 1030 cm^{-1}, gradually disappeared showing the complete removal of the methoxy functional groups from the substituted aromatic rings in both trapped and deposited products. Similar behavior was reported during conventional pyrolytic char formation of lignin [21]. These results, along with the results indicating the formation of soot particulates detected by FTIR from outlet neck and top wall of the LPHP reactor (Figure 4), are consonant with literature data on conventional pyrolysis of lignin and cellulose at high temperatures [21,22].

GPC measurements described below were performed to analyze further the content and behavior of trapped products not detectable by GC-MS.

3.3. Molecular Weight Distribution of the Lignin Homogeneous Pyrolysis Products

3.3.1. GPC Analysis

To better understand the nature of the hydrolytic lignin gas-phase depolymerization process during homogeneous pyrolysis in LPHP reactor, gel permeation chromatography (GPC) was employed to examine the molecular weight distribution of products. The results are shown in Figure 5 for initial lignin (HL) in comparison with depolymerized lignin (PHL) at various laser powers.

These GPC spectra show the various fractions of the hydrolytic lignin and how they change as the lignin structure is deconstructed during depolymerization. As the temperature of the pyrolysis increases, the summits of these fractions move toward lower molecular weights while the new peaks,

 doi:10.20944/preprints202504.0455.v1

indicating the new fragments, are also formed and intensified subsequently. Even though the GPC is the most common method to determine molecular weight distribution by many researchers, this technique has a major drawback. Obtained by this method Mw values are relative to other compounds such as polystyrene. Thus, one cannot draw a definite conclusion based on the values reported in Table 2. The weight average molecular weights (M_w), the number average molecular weights (M_n) and the polydispersity indexes (PDI) of the initial lignin, as well as the generated products after pyrolysis are provided for comparison purposes.

The molecular weight values of intact lignin sample, M_n and M_w of 1397 and 5591 g/mol, respectively, are significantly higher than those for the rest of the pyrolyzed sample, indicating on more efficiency of the homogeneous pyrolysis in the gas phase in depolymerization of hydrolytic lignin. It is also evident that by increasing the laser power, these values reduce gradually as a result of the increased pyrolysis temperature.

Table 2. The weight-average (M_w) and number-average (M_n) molecular weights of lignin and pyrolyzed lignin.

	HL	PHL20	PHL30	PHL40	PHL50	PHL60
M_w (g/mol)	5591	2298	1985	1947	1601	763
M_n (g/mol)	1397	614	325	309	354	113
PDI	4.0	3.7	6.1	6.3	5.1	6.7

Furthermore, the polydispersity index (PDI) of the intact lignin is lower than that of all the pyrolyzed samples except PHL20 sample, pyrolyzed at 20% of maximum laser power. Collectively, these results suggest that the lignin macromolecules are broken down into smaller fragments and spread over a broader range of molecular weight values, Figure 5.

This observation is at variance with reports in literature on the effect of temperature on molecular weight of pyrolytic lignin [23–25]. Based on the reviewed studies, an increasing trend in the molecular weight distribution, as determined by GPC, was observed with higher pyrolysis temperatures for kraft lignin, organosolv lignin, spruce organosolv lignin, wheat straw organosolv lignin, and milled pine wood lignin. Ragauskas and Ben, for instance, observed that the molecular weights are increased with increasing pyrolysis temperature for both fast and slow pyrolysis oils produced from pine wood [23]. Kersten *et al.* explained this phenomenon in terms of the interplay of chemistry and mass transport [24]. They reported heavier bio-oil recovery during pyrolysis, regardless of the lignin type, by increasing temperature due to the higher escape rate of heavier components from the reacting region, as well as the low partial pressure.

In fact, lignin macromolecules undergo fragmentation during homogeneous gas phase processes in the LPHP reactor, which seem to indicate that products in other reactors are involved in the secondary repolymerization reactions, which increase the Mw of the final products. It is pertinent to mention that both ESI–MS and GPC results on the primary pyrolysis products of organosolv lignin at temperatures between 360 and 700 °C show a negligible effect of the pyrolysis temperature on the molar weight distribution using an original vacuum screen heater [26].

 doi:10.20944/preprints202504.0455.v1

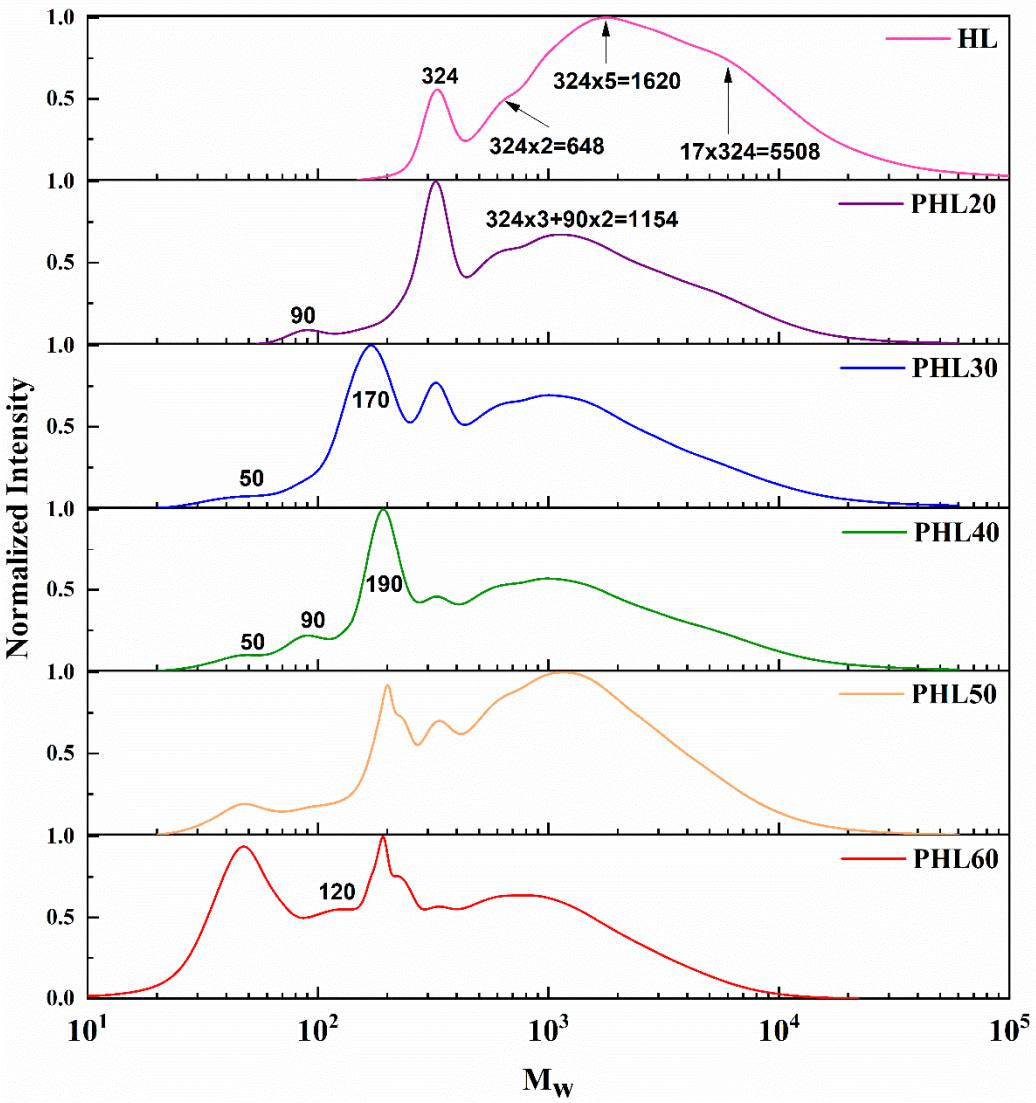

Figure 5. GPC spectra for initial HL vs products from HL pyrolysis (collected in the trap) at various laser powers in LPHP reactor; 20% (14.7W), 30% (21.8W), 40% (28 W), 50% (33.5W), 60% (38 W).

3.3.2. The Radical Character of the Decomposition of Lignin in LPHP Reactors

A dramatic new environment for pyrolysis of HL in LPHP reactor excluding direct contact between volatiles and residue chars lead to the principal simplification of the primary decomposition processes of the lignin macromolecules. As a result, the major fraction of the pyrolysis products (~ 80%, w) represents a mixture of the initial intact HL and its depolymerized fragments - oligomers and oligomer radicals, as described in the current work and mentioned in refs [2,3]. The converted lignin (~ 10-15%, w) deposited on the cold areas, outside of the reactor, shows high content of radicals, Figure 6. The low g values of the detected radicals from the neck of the countercurrent reactor equal to 2.0029 and 2.0028 confirms the removal of most of the lignin functional groups containing polar groups by formation of "naked" soot-like conjugated substances; a notable change of the g values of the intrinsic radicals (2.0043, initial lignin, inset, Figure 6) occurs.

 doi:10.20944/preprints202504.0455.v1

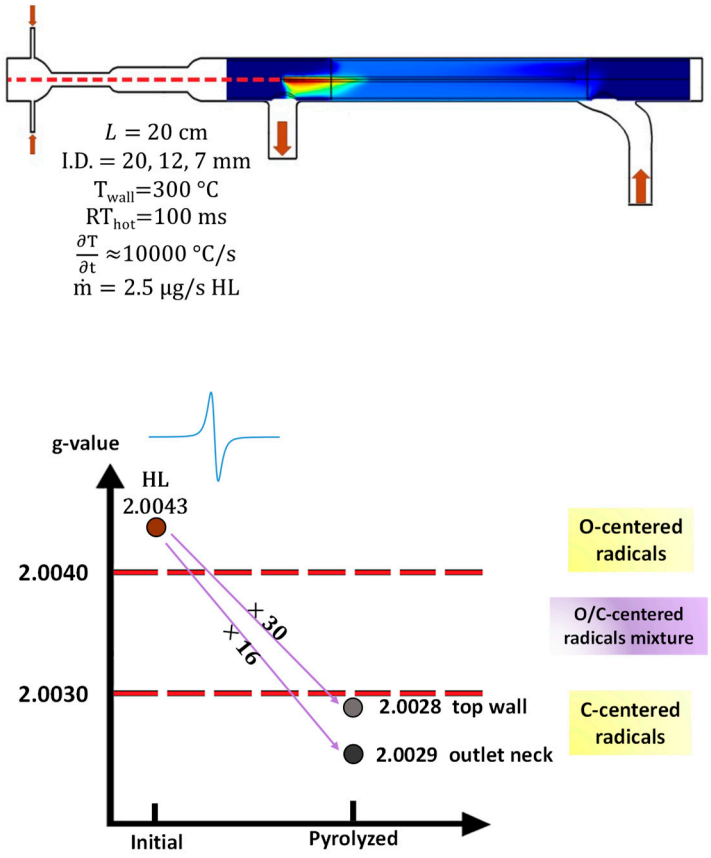

Figure 6. Brown deposits (g-value of 2.0029) on the reactor outlet neck with x16 higher EPR signal intensity than that in initial HL. Black deposits (g-value of 2.0028) on the reactor top wall with x30 higher intensity (at 28W of laser power) than in HL. The g-values 2.0030 and 2.0040 on the Y-axis are arbitrary marker values for C-, O-centered radicals, respectively, as well as a mixture of these radicals between these values.

Generally, the presence of the macro- radicals provides strong binding conditions to develop initial clusters of PAHs [27].

3.4. Formation Mechanism of PAHs from HL Gas-Phase Pyrolysis in LPHP Reactor.

3.4.1. Combustion Related Homogeneous Channels for Formation of PAHs

The formation of PAHs and soot particulates (Figures 3 and 4) from lignin gas-phase decomposition in LPHP reactor can be explained within the traditional multizone soot particulates formation mechanism in hydrocarbon flames. In the pre-flame zone, the fuel or combustible precursors are vaporized at temperatures ranging from ambient up to about 1200ºC. In the flame zone where temperature exceeds 1200ºC the fuel species undergo complete combustion; this zone is associated with the formation of soot and other organic pollutants. The molecular growth of PAHs and soot inception occurs in the post -flame zone with decreased temperatures ranging from 1200 to 600ºC. Below 600ºC, the soot inception/formation rate is exceedingly low.

The possible mechanisms relevant to the aromatics growth and PAHs/soot particulate formation have been actively disputed in literature over the last three decades. The current primary focus is the generation of the first few aromatic rings out of small aliphatic compounds. This is perceived by many to be a rate-limiting stage in the reaction sequence leading to larger aromatics, and it is commonly accepted that the formation of the first aromatic ring is the kinetic bottleneck in the soot formation chain [27,28]. Subsequent growth of PAHs from a single aromatic species can proceed via a repetitive sequence of hydrogen abstraction and acetylene addition reactions (seminal **HACA** mechanism) [27–29]

 doi:10.20944/preprints202504.0455.v1

Various mechanisms on the formation of PAHs at high temperatures are also largely discussed in literature [30–34]. In particular, an aryl-aryl combination [35], phenyl or methyl addition/cyclization [36], and others (see detail discussion in supporting information, Section 4) have also been reported.

The formation of naphthalene [3] and its derivatives directly observed in LPHP reactor, Figure 3, suggests the importance of its formation channels - reaction (1) (and reaction (3) in supporting information, Section 4)

$$\mathbf{2\ C_5H_5 \rightarrow C_{10}H_8 + 2H} \quad (1)$$

involving a key, cyclopentadienyl, C_5H_5 (CPD)[37,38], and naphthalenyl radicals [39].

The formation of CPD radicals from pyrolysis/oxidation reactions of numerous lignin contracted models (aromatics) such as catechol, hydroquinone, and phenol has been shown in our early publications [40–42], and more recently [43], suggested to occur during pyrolysis of p-coumaryl alcohol at elevated temperatures, > 700 ºC, Figure S3. The expulsion of CO from phenoxy rings is typically considered to lead to the formation of cyclopentadienyl and hydroxy-cyclopentadienyl radicals particularly from pyrolysis of catechol, hydroquinone [44], guaiacol [45], and para-coumaryl alcohol [43]. Further recombination of such radicals form naphthalene, indene, hydroxy indene and other derivatives, as experimentally established in isothermal reactors. [44,46]

The role of the resonance-stabilized cyclopentadienyl and other aromatic radicals in soot formation has also been indirectly demonstrated recently during pyrolysis/oxidative pyrolysis of the 1-methylnaphthalene at ~ 1100°C in two-sections tubular combustion reactor [47]. It should be noted that the CPD radicals are more stable than phenoxy radicals at such high temperatures (> 700 -1000 °C) [41]. Accordingly, the ratio [CPD]/[PhO] =2.0 at 700 °C was suggested to increase to 88.4 at 1000 °C in a numerical modeling study using a known scheme of phenol pyrolysis reactions analyzed in detail in the same publication[41]. The formation of derivatized CPD radicals from lignin key models and monomers, particularly para-coumaryl alcohol at elevated temperatures, has been justified theoretically by Asatryan et al based on the first-principles analysis of reaction mechanisms [48] (detailed in the supporting information, Figure S4,).

Thus, due to the flash heating at elevated temperatures and intense de-functionalization of lignin macromolecule (intermediate oligomers), the formation, and further reactions of CPD radicals can occur described in Scheme 1 (and Figure S5). In other words, the naphthalene formation initiates generation and growth of the myriads of low molecular weight (LMW) PAHs (Figure 3), both benzenoid (phenanthrene, pyrene, etc.) and cyclopentane-based fused (acenaphthylene, fluoranthene, etc.) PAH structures through both HACA mechanism, and/or addition of the new cyclopentadienyl radicals, [28,49–51] as summarized in Figure S5.

 doi:10.20944/preprints202504.0455.v1

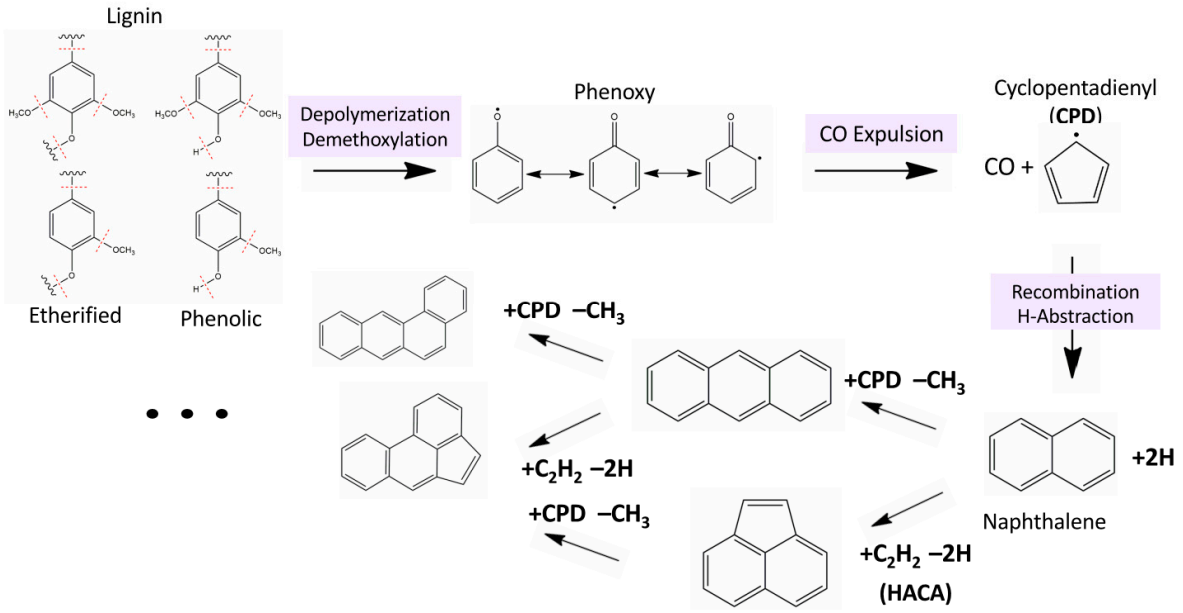

Scheme 1. Mechanistic homogeneous pathway of PAHs formation during high temperature gas-phase pyrolysis of lignin.

The detailed analysis of the formation of soot particulates from LPHP using ESI MS and LDI MS techniques is underway, while similar results from CA reactor on detection of soot particulates up to 2000-2500 g/mol after pyrolysis of lignin dispersed into gas phase in isothermal conditions is already reported. [2]

3.4.2. A "Heterogenous" Mechanism for Formation of PAHs

As it was mentioned above, we did not detect any phenolics from co-current and counter-current LPHP reactors in the entire range of laser power from 20 to 38W. Therefore, it could be concluded that phenolics do not form in these conditions (decomposition reactions, particularly CO expulsion from a phenoxyl-type radical being dominant over hydrogen abstraction reactions, which lead to phenolics), and they rapidly convert into PAHs and soot particulates at elevated temperatures, as soon as they are formed (≥ 900-1000 °C, Figure 2), Section 3.4.1 above.

An alternative possibility is a heterogeneous formation of PAHs that also involves CPD radicals. The phenoxyl radicals released from destruction of lignin macromolecules (Scheme 1) stay trapped between polar lignin sub-units, and further expulsion of CO from phenoxy unit leads to the formation of adsorbed on the lignin macromolecule CPD radicals (CPDa). Consequently, the surface reactions of CPDa (due to their known higher mobility; see supporting information, Section 6) could produce PAHs via a scenario described in Scheme 1 (Figure S5).

One could assume a similar mobility of the adsorbed and stabilized CPDa radicals on the surface of the HL macromolecule (as discussed in Supporting Information, Section 6), perhaps to a lesser extent due to the polar nature of the lignin branches; the formation of naphthalene, according to reaction (1), can be envisioned at elevated temperatures.

Evidence on formation of the of immobilized CPD radicals into the lignin lattice: Evidence of embedded CPD radicals (CPDa) on lignin matrix has been provided in our early pyroprobe fast fractional pyrolysis experiments on lignin [52]. The products released at different temperatures in fast flow of nitrogen gas were collected on Cambridge filter (CF) at room temperature (Figure S6) and subjected to EPR analysis, Figure 7a. A registered structureless EPR line with g = 2.0051 at 300 °C set-temperature is slowly transformed into a well-resolved complex EPR spectra with an increase of the pyrolysis temperature up to 600 °C. The EPR spectra seems to be a superposition of EPR signals of several paramagnetic species. Further increase of temperature to 700 °C leads to the distortion of the

 doi:10.20944/preprints202504.0455.v1

well resolved spectrum at 600 °C with g = 2.0061 at the center to generate another signal with lower g= 2.0039. A trend can be traced in conversion into the single line at temperatures higher than 700 °C. A benchmark EPR line at g = 1.9932 from top spectra in Figure 7(a) is compared with the reference EPR spectrum of pure CPD generated from vacuum pyrolysis of tricarbonylcyclo-pentadienylmanganese (Figure S3 [43,53]), black line in Figure 7(b). The line at g = 1.9932 of CPD radical doesn't overlay with any other EPR lines of an organic radical generated from vacuum pyrolysis of a number of lignin model compounds to provide evidence on presence of CPD radicals [53]. Importantly, it exactly fits with the same line for the radicals generated from vacuum pyrolysis of p-coumaryl alcohol (green line in Figure 7(b)) and identified as traces of CPD after annihilation of the radical mixture [43], Figure S3. Therefore, the immobilization of CPD radicals on a lignin matrix appears feasible, and the subsequent reactions of these adsorbed radicals, as discussed above, may be highly relevant.

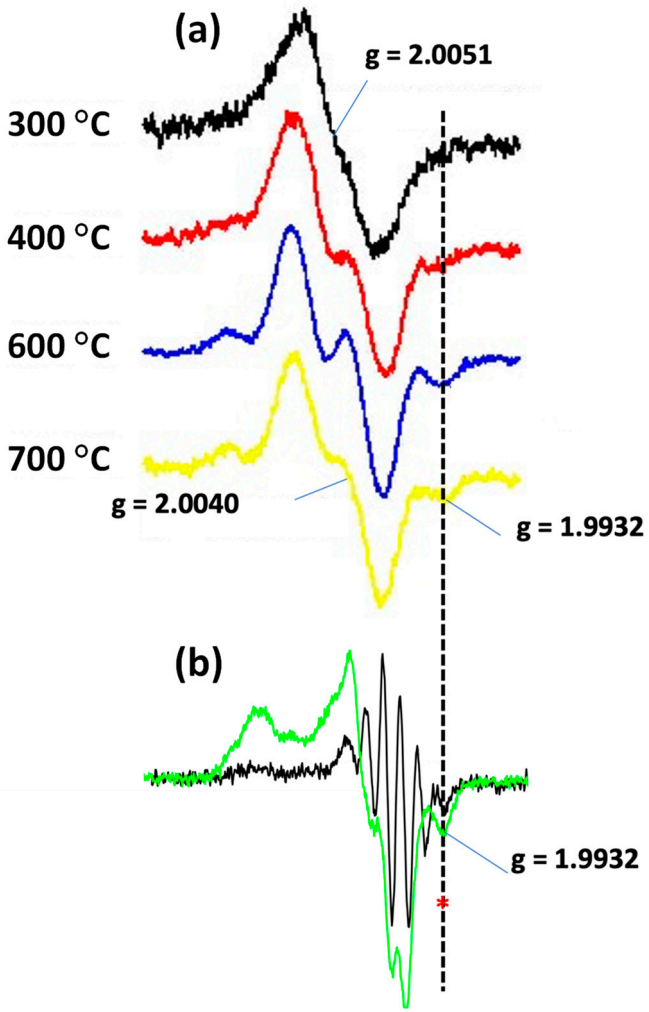

Figure 7. (a) - Top four EPR spectra were detected at room temperature from lignin pyrolysis in pyroprobe at 300 ºC (black), 400 ºC (red), 600 ºC (blue) and 700 ºC (yellow) set temperatures. Radicals were accumulated in Cambridge filter. (b) - Two spectra below present a reference EPR spectrum from vacuum pyrolysis of tricarbonylcyclopentadienylmanganese (black line, reaction (1) in Figure S3) overlayed with the radicals EPR spectrum detected from vacuum pyrolysis of p-coumaryl alcohol at elevated temperatures (>700 oC); both spectra were detected at liquid N2 temperature. Red asterisk shows the reference line from CPD radical at g = 1.9932.

 doi:10.20944/preprints202504.0455.v1

In summary, the reaction sequences presented in Scheme 1 (Figure S5) up to generation of LMW PAHs may occur both homogeneously in the gas phase, as well as heterogeneously on the surface of the macromolecules of HL.

4. Conclusions

Fast pyrolysis of hydrolytic lignin (HL) dispersed in the gas phase was performed in IR CO_2 laser powered homogeneous pyrolysis (LPHP) reactor. Lignin breaks down to fragments and forms GC-MS detectable PAHs (MW<300 Da). The phenolic compounds were not observed among products at higher than ~20 W non-focused laser power conditions. GPC analysis revealed a partial fragmentation of HL (at ~ 10-15% conversion) deposited on the cold area of the LPHP reactor. PAHs and soot-like substances were dominant components of the deposits at higher than 20-22W laser powers. The dominant fraction of lignin (~ 80%) transported through the hot zone consists of the decomposed neutral fragments, oligomer radicals, and non-reacted intact macromolecules of lignin.

A traditional combustion chemistry mechanism relevant to the soot formation in hydrocarbon flames at elevated temperatures was applied to explain the formation of PAHs under laser irradiation involving formation and reactions of CPD radicals. An alternative, "heterogenous" pathway for generation of PAHs (parallel to the homogeneous pathways) is also proposed involving reactions of adsorbed on HL macromolecules CPDa radicals.

Supplementary Materials: The following supporting information can be downloaded at the website of this paper posted on Preprints.org.

Acknowledgements: This work was funded by National Science Foundation CBET #1805677 with partial support from the National Science Foundation EPSCoR program (OIA #1632854) and USDA NIFA Hatch Program (LAB #94443). Published with the approval of the Director of the Louisiana Agricultural Experiment Station as manuscript #2022-232-38298.

References

1. Barekati-Goudarzi, M.; Boldor, D.; Marculescu, C.; Khachatryan, L. Peculiarities of Pyrolysis of Hydrolytic Lignin in Dispersed Gas Phase and in Solid State. *Energy & Fuels* **2017**, *31*, 12156-12167, doi:10.1021/acs.energyfuels.7b01842.
2. Barekati-Goudarzi, M.; Boldor, D.; Khachatryan, L.; Lynn, B.; Kalinoski, R.; Shi, J. Heterogeneous and Homogeneous Components in Gas-Phase Pyrolysis of Hydrolytic Lignin. *Acs Sustain Chem Eng* **2020**, *8*, 12891-12901, doi:10.1021/acssuschemeng.0c03366.
3. Khachatryan, L.; Barekati-Goudarzi, M.; Kekejian, D.; Aguilar, G.; Asatryan, R.; Stanley, G.G.; Boldor, D. Pyrolysis of Lignin in Gas-Phase Isothermal and cw-CO2 Laser Powered Non-Isothermal Reactors. *Energ Fuel* **2018**, *32*, 12597-12606, doi:10.1021/acs.energyfuels.8b03312.
4. D. Kekejian; L. Khachatryan; M. Barekati-Goudarzi; Boldor., D. Implication of COMSOL to Laser Powered Non-Isothermal Reactors for Pyrolysis in the Gas Phase. *COMSOL CONFERENCE* **2018**, Boston Marriott Newton, October 3-5.
5. Thomas McGrath, R.S., Mohammad Hajaligol*. An experimental investigation into the formation of polycyclic-aromatic hydrocarbons(PAH) from pyrolysis of biomass materials. *Fuel* **2001**, *80*, 1787-1797.
6. Fabbri, D.; Adamiano, A.; Torri, C. GC-MS determination of polycyclic aromatic hydrocarbons evolved from pyrolysis of biomass. *Anal Bioanal Chem* **2010**, *397*, 309-317, doi:10.1007/s00216-010-3563-5.
7. Kozliak, E.I.; Kubatova, A.; Artemyeva, A.A.; Nagel, E.; Zhang, C.; Rajappagowda, R.B.; Srnirnova, A.L. Thermal Liquefaction of Lignin to Aromatics: Efficiency, Selectivity, and Product Analysis. *Acs Sustain Chem Eng* **2016**, *4*, 5106-5122, doi:10.1021/acssuschemeng.6b01046.
8. Westerholm, R.N.; Alsberg, T.E.; Frommelin, A.B.; Strandell, M.E.; Rannug, U.; Winquist, L.; Grigoriadis, V.; Egeback, K.E. Effect of Fuel Polycyclic Aromatic Hydrocarbon Content on the Emissions of Polycyclic Aromatic-Hydrocarbons and Other Mutagenic Substances from a Gasoline-Fueled Automobile. *Environmental Science & Technology* **1988**, *22*, 925-930, doi:DOI 10.1021/es00173a010.

 doi:10.20944/preprints202504.0455.v1

9. de Souza, C.V.; Corrêa, S.M. Polycyclic aromatic hydrocarbons in diesel emission, diesel fuel and lubricant oil. *Fuel* **2016**, *185*, 925-931, doi:10.1016/j.fuel.2016.08.054.
10. Zhou, H.; Wu, C.F.; Onwudili, J.A.; Meng, A.H.; Zhang, Y.G.; Williams, P.T. Polycyclic Aromatic Hydrocarbon Formation from the Pyrolysis/Gasification of Lignin at Different Reaction Conditions. *Energy & Fuels* **2014**, *28*, 6371-6379, doi:10.1021/ef5013769.
11. Smith, E.A.; Lee, Y.J. Petroleomic Analysis of Bio-oils from the Fast Pyrolysis of Biomass: Laser Desorption Ionization−Linear Ion Trap−Orbitrap Mass Spectrometry Approach. *Energy & Fuels* **2010**, *24*, 5190-5198, doi:10.1021/ef100629a.
12. Shaub, W.M.; Bauer, S.H. Laser-Powered Homogeneous Pyrolysis. *Int J Chem Kinet* **1975**, *7*, 509-529.
13. Kubat, P.; Pola, J. Spatial Temperature Distribution in Cw Co2-Laser Photosensitized Reactions. *Collect Czech Chem C* **1984**, *49*, 1354-1359.
14. Molin, Y.N.; Panfilov, V.N.; Petrov, A.K. Infrared Photochemistry. *Novosibirsk, Izd. Nauka* **1985**.
15. Sukiasyan, A.A.; Khachatryan, L.A.; Il'in, S.D. Measuring of the kinetic parameters of homogeneous decomposition of Azomethane under CO_2-laser irradiation *Arm.Khim.Zhur.* **1988**, *41*, 104.
16. Russell, D.K. Infrared-Laser Powered Homogeneous Pyrolysis. *Chem Soc Rev* **1990**, *19*, 407-437.
17. Mantashyan, A.A. Peculiarities of the slow combustion of a hydrocarbon in a "wall-less" reactor with laser heating. *Combust Flame* **1998**, *112*, 261-265.
18. Swihart, M.T.; Carr, R.W. Pulsed laser powered homogeneous pyrolysis for reaction kinetics studies: Probe laser measurement of reaction time and temperature. *Int J Chem Kinet* **1996**, *28*, 817-828, doi:Doi 10.1002/(Sici)1097-4601(1996)28:11<817::Aid-Kin4>3.3.Co;2-Y.
19. Todorciuc, T.; Capraru, A.-M.; Kratochvilova, I.; Popa, V.I. Characterization of non-wood lignin and its hydroxymethylated derivatives by spectroscopy and self-assembling investigations. . **2009**, *43*, 399-408.
20. Faix, O. Classification of Lignins from Different Botanical Origins by FT-IR Spectroscopy. **1991**, *45*, 21, doi:https://doi.org/10.1515/hfsg.1991.45.s1.21.
21. Sharma, R.K., Wooten, J. B., Baliga, V. L., Lin, X., Chan, W. G., Hajaligol, M. R. Characterization of chars from pyrolysis of lignin. *Fuel* **2004**, *83*, 1469-1482.
22. Boon, J.; Bobeldijk Pastorova, I.; Botto, R.E.; Arisz, P. Structural studies on cellulose pyrolysis and cellulose chars by PYMS, PYGCMS, FTIR, NMR and by wet chemical techniques. *Biomass and Bioenergy* **1994**, *7*, 25-32, doi:10.1016/0961-9534(94)00044-T.
23. Ben, H.; Ragauskas, A.J. Comparison for the compositions of fast and slow pyrolysis oils by NMR characterization. *Bioresource Technology* **2013**, *147*, 577-584, doi:https://doi.org/10.1016/j.biortech.2013.07.151.
24. Marathe, P.S.; Westerhof, R.J.M.; Kersten, S.R.A. Fast pyrolysis of lignins with different molecular weight: Experiments and modelling. *Applied Energy* **2019**, *236*, 1125-1137, doi:https://doi.org/10.1016/j.apenergy.2018.12.058.
25. Zhou, S.; Garcia-Perez, M.; Pecha, B.; Kersten, S.R.A.; McDonald, A.G.; Westerhof, R.J.M. Effect of the Fast Pyrolysis Temperature on the Primary and Secondary Products of Lignin. **2013**, *27*, 5867-5877, doi:10.1021/ef4001677.
26. Zhou, S.; Garcia-Perez, M.; Pecha, B.; Kersten, S.R.A.; McDonald, A.G.; Westerhof, R.J.M. Effect of the Fast Pyrolysis Temperature on the Primary and Secondary Products of Lignin. *Energy & Fuels* **2013**, *27*, 5867-5877, doi:Doi 10.1021/Ef4001677.
27. Wang, H. Formation of nascent soot and other condensed-phase materials in flames. *P Combust Inst* **2011**, *33*, 41-67, doi:10.1016/j.proci.2010.09.009.
28. Frenklach, M.; Gardiner, W.C.; Stein, S.E.; Clary, D.W.; Yuan, T. Mechanism of Soot Formation in Acetylene-Oxygen Mixtures. *Combustion Science and Technology* **1986**, *50*, 79-115, doi:10.1080/00102208608923927.
29. Frenklach, M.; Singh, R.I.; Mebel, A.M. On the low-temperature limit of HACA. *P Combust Inst* **2019**, *37*, 969-976, doi:10.1016/j.proci.2018.05.068.
30. Saggese, C.; Frassoldati, A.; Cuoci, A.; Faravelli, T.; Ranzi, E. A wide range kinetic modeling study of pyrolysis and oxidation of benzene. *Combust Flame* **2013**, *160*, 1168-1190, doi:https://doi.org/10.1016/j.combustflame.2013.02.013.

 doi:10.20944/preprints202504.0455.v1

31. Ledesma, E.B.; Marsh, N.D.; Sandrowitz, A.K.; Wornat, M.J. Global kinetic rate parameters for the formation of polycyclic aromatic hydrocarbons from the pyrolyis of catechol, a model compound representative of solid fuel moieties. **2002**, *16*, 1331-1336, doi:10.1021/ef010261.
32. Mastral, A.M.; Callen, M.S. A review an polycyclic aromatic hydrocarbon (PAH) emissions from energy generation. **2000**, *34*, 3051-3057, doi:10.1021/es001028d.
33. Akazawa, M.; Kojima, Y.; Kato, Y. Formation mechanism of polycyclic compounds from phenols by fast pyrolysis. *EC Agriculture* **2015**, *1*, 67-85.
34. Zhou, H.; Wu, C.; Onwudili, J.A.; Meng, A.; Zhang, Y.; Williams, P.T. Polycyclic Aromatic Hydrocarbon Formation from the Pyrolysis/Gasification of Lignin at Different Reaction Conditions. *Energy & Fuels* **2014**, *28*, 6371-6379, doi:10.1021/ef5013769.
35. A.F. Sarofim; J.P. Longwell; M.J. Wornat; J. Mukherjee; (Ed.), i.H.B. Soot Formation in Combustion. *Springer-Verlag, Berlin* **1994**.
36. B. Shukla; Koshi, M. Comparative study on the growth mechanisms of PAHs. *Combust Flame* **2011**, *158*, 369–375.
37. Lu, M., Mulholland, J.A. *Chemosphere* **2001**, *42*, 623.
38. Yang, B.; Hu, B.; Koylu, U.O. Mean soot volume fractions in turbulent hydrocarbon flames: A comparison of sampling and laser measurements. *Combustion Science and Technology* **2005**, *177*, 1603-1626, doi:Doi 10.1080/00102200590959233.
39. Chu, T.C.; Smith, M.C.; Yang, J.; Liu, M.J.; Green, W.H. Theoretical study on the HACA chemistry of naphthalenyl radicals and acetylene: The formation of C12H8, C14H8, and C14H10 species. *Int J Chem Kinet* **2020**, *52*, 752-768, doi:10.1002/kin.21397.
40. Khachatryan, L.; Adounkpè, J.; Maskos, Z.; Dellinger, B. Formation of Cyclopentadienyl Radical from the Gas-Phase Pyrolysis of Hydroquinone, Catechol, and Phenol. *Environmental science & technology* **2006**, *40*, 5071-5076, doi:10.1021/es051878z.
41. Khachatryan, L.; Adounkpe, J.; Dellinger, B. Formation of Phenoxy and Cyclopentadienyl Radicals from the Gas-Phase Pyrolysis of Phenol. *The Journal of Physical Chemistry A* **2008**, *112*, 481-487, doi:10.1021/jp073999m.
42. Lavrent Khachatryan; Meng-xia Xu; Ang-jian Wu; Mikhail Pechagin; Asatryan, R. Radicals and Molecular Products from the Gas-Phase Pyrolysis of Lignin Model Compounds. Cinnamyl Alcohol. *J. Anal.Appl.Pyr* **2016**, DOI: 10.1016/j.jaap.2016.1007.1004, doi:10.1016/j.jaap.2016.07.004.
43. Meng-xia Xu; Lavrent Khachatryan; Alexander Baev; Asatryan, R. Radicals from the Gas-Phase Pyrolysis of Lignin Model Compounds. p-Coumaryl Alcohol *RSC Adv.* **2016**, *6*, 62399-62405, doi:10.1039/C6RA11372A.
44. Julien Adounkpe; Martin Aina; Daouda Mama, a.; Sinsin, B. Gas Chromatography Mass Spectrometry Identification of Labile Radicals Formed during Pyrolysis of Catechool, Hydroquinone, and Phenol through Neutral Pyrolysis Product Mass Analysis. *Hindawi Publishing Corporation; ISRN Environmental Chemistry* **2013**, *Article ID 930573*, doi:10.1155/2013/93057.
45. Custodis, V.B.F.; Hemberger, P.; Ma, Z.Q.; van Bokhoven, J.A. Mechanism of Fast Pyrolysis of Lignin: Studying Model Compounds. *J Phys Chem B* **2014**, *118*, 8524-8531, doi:10.1021/jp5036579.
46. Mulholland, J.A., Lu, M. and Kim, D.H. Pyrolytic growth of polycyclic aromatic hydrocarbons by clyclopentadienyl moieties. *Proc. Combust. Inst.* **2000**, *28*, 2593-2599.
47. Herring, P.; Khachatryan, L.; Lomnicki, S.; Dellinger, B. Paramagnetic centers in particulate formed from the oxidative pyrolysis of 1-methylnaphthalene in the presence of Fe(III)(2)O-3 nanoparticles. *Combust Flame* **2013**, *160*, 2996-3003, doi:10.1016/j.combustflame.2013.06.025.
48. Asatryan, R.; Bennadji, H.; Bozzelli, J.W.; Ruckenstein, E.; Khachatryan, L. Molecular Products and Fundamentally Based Reaction Pathways in the Gas-Phase Pyrolysis of the Lignin Model Compound p-Coumaryl Alcohol. *J Phys Chem A* **2017**, *121*, 3352-3371, doi:10.1021/acs.jpca.7b01656.
49. Shukla, B.; Koshi, M. A novel route for PAH growth in HACA based mechanisms. *Combust Flame* **2012**, *159*, 3589–3596, doi:10.1016/j.combustflame.2012.08.007.

 doi:10.20944/preprints202504.0455.v1

50. Bockhorn, H.; Fetting, F.; Wenz, H. Investigation of the Formation of High Molecular Hydrocarbons and Soot in Premixed Hydrocarbon-Oxygen Flames. *Berichte der Bunsengesellschaft für physikalische Chemie* **1983**, *87*, 1067-1073, doi:10.1002/bbpc.19830871121.
51. Frenklach, M.; Warnatz, J. Detailed Modeling of PAH Profiles in Sooting Low-Pressure Acetylene Flame. *Combustion Science and Technology - COMBUST SCI TECHNOL* **1987**, *51*, 265-283, doi:10.1080/00102208708960325.
52. Lavrent Khachatryan; Zofia Maskos, a.; Dellinger., B. The Tar and Tar Radicals from Lignin Pyrolysis. . *SFRBM (Society for Free Radical Biology and Medicine)* **2014**, *November 19-23*.
53. Khachatryan, L., Adounkpe, J., and Dellinger, B. Formation of Phenoxy and cyclopentadienyl radicals from the gas-phase pyrolysis of phenol. *J.Phys.Chem., A* **2008**, *112*, 481-487.